IEEE Access
Multidisciplinary | Rapid Review | Open Access Journal

Received April 10, 2020, accepted May 24, 2020, date of publication June 2, 2020, date of current version June 16, 2020.

Digital Object Identifier 10.1109/ACCESS.2020.2999465

Modeling Multi-Layer OHL Conductors Undergoing Wind-Induced Motion

MOHAMMED A. ALAQIL, (Member, IEEE), AND KONSTANTINOS KOPSIDAS, (Senior Member, IEEE)
Department of Electrical and Electronic Engineering, The University of Manchester, Manchester M13 9PL, U.K.

Corresponding author: Mohammed A. AlAqil (m.alaqil@manchester.ac.uk)

This work was supported by the King Faisal University, Saudi Arabia, on behalf of the Saudi Ministry of Education and The University of Manchester, U.K.

ABSTRACT Utilities aim to improve asset management strategies and enhance the utilization of their assets through low-risk reliable practices. Overhead lines and conductor designs have been evolving to increase systems' power capacity and mechanical integrity, which have also extended asset lifetimes. Nevertheless, it is still challenging to predict a conductor's fatigue stresses due to wind-induced vibrations that can help to estimate its useful life. A finite element model (FEM) has been established in COMSOL to study the free and forced wind-induced vibrations and the resultant fatigue on single multi-layer conductors considering their complex round and trapezoidal stranding patterns. The FEM analysis is based on multi-physics accounting for the conductor's thermal and mechanical aspects as well as material and geometry properties. Consequently, the fatigue is quantified for both inter-layer and inter-wire interactions. The simulations show that free conductor vibrations are dictated by the conductor materials and tension distribution between the core and aluminum strands. The bigger the difference between the material properties of the core and aluminum, the lesser the conductor vibrations, especially when the aluminum becomes slack. In fact, a conductor equipped with carbon core (ACCC), has the best vibration resistance among other conductors with steel core (ACSR) and homogeneous (AAACs). Forced vibration simulations identified non-linear fatigue stresses for round and trapezoidal designs, which is more pronounced in larger conductor sizes. Larger trapezoidal ACSRs exhibit better fatigue resistance compared to smaller and round stranded AAACs.

INDEX TERMS ACSR, aeolian vibration, conductors, fatigue, FEM, HTLS, overhead lines, uprating.

I. INTRODUCTION

The power and energy sectors are undertaking strategic transformations to achieve the milestones of electrification and reduction in dispatching fossil-fueled energy sources. Such transformation entails connecting high-shares of clean energy sources into the bulk electrical network causing a swift increase in the power transferred within OHL corridors [1], [2]. This is an inevitable result of the continuous growth of connected renewables into the power networks and renewable energy strategies targeting the electrification of heat and transport to comply with low carbon emission policies [3]–[6].

Traditionally, utilities are obliged to enforce network expansion by building new overhead lines (OHLs). However, this expansion solution is expensive and frequently require permission to be allocated the proper right-of-way (ROW). This lengthy procedure involves, among other design and regulation approvals, gaining social acceptance of the OHL to ensure visual amenity and environmental compliance.

To avoid such complicated procedures, utilities seek out more flexible, economic, and faster-to-implement reinforcement methods. Such reinforcement can be achieved by re-conductoring the existing OHL with bigger size conductors or utilizing conductors that feature new technologies such as High-Temperature Low-Sag (HTLS). The latter enables safe operation at higher (than ACSR) temperatures [7].

Utilities are required to maintain assets operation and aim to enhance their lifetime by optimizing their design and planning maintenance, which require understanding asset ageing mechanisms and end-of-life predictions [7]. In most cases, where corrosion degradation is not an issue, the

The associate editor coordinating the review of this manuscript and approving it for publication was Ildiko Peter.

OHL conductor ageing and risk of fatal failure are mainly attributed to wind-induced energy that causes conductor motions. The OHL-conductor system is susceptible to wind-induced motions that impact the integrity of the conductor as well as the line's structure (i.e., pylons or wood poles). In fact, the exposure of conductors to wind-induced vibrations is a dominant constraint that limits their installation tension. One of the most destructive wind-induced motions is aeolian vibrations, which is the primary cause of conductor strands damage and often determines the long-term ageing mechanism and its life expectancy. Therefore, conductors suffer from wind-induced fatigue due to inter-layer and inter-wire interactions.

Advancements in conductor technologies led to conductor designs that are classified by their installation procedure, geometrical shape, and material properties. The existing standards used to evaluate OHL conductor's mechanical (i.e. vibration) and electrical (i.e. thermal) performance implement simplified conductor geometry models using its overall (i.e., homogeneous) properties [8]–[10]. Although standard practices provide good results, further assessment is necessary to differentiate the performance of the different sizes and types of diverse single-layer and multi-layer conductor technologies.

This paper presents a multi-physics Finite Element Modelling (FEM) approach based on COMSOL to simulate the structural dynamics of OHL conductors undergoing aeolian vibration. The FEM approach permits studying the conductor's free and forced vibrations considering its inter-layer and inter-wire interactions. Furthermore, the paper quantifies the effect of over-simplifying the conductor complex geometry.

The next section summarizes the existing conductor vibration models and their associated standard guidelines. The presented FEM approach is detailed and validated is section III. The free vibration response and fatigue stresses are simulated and verified using the FEM approach for various conductor sizes and types in sections IV and V, respectively. The FEM approach is extended in section V to examine vibration fatigue stresses exerted on trapezoidal conductor strands. Conclusions and suggested future work are reported in VI.

II. BACKGROUND ON CONDUCTOR VIBRATION AND FATIGUE MODELLING

A. CONDUCTOR FREE VIBRATION CALCULATIONS

The OHL conductor vibrations have been investigated for decades with efforts to quantify aeolian vibrations which resulted in the Energy Balance Method (EBM) [11]–[14]. Conductor modelling is a major task in the formulation of the conductor vibrations dynamics within the EBM, which constitute the appropriateness of the formulated solution.

The string and beam models have been implemented to represent the conductor geometry and response. On the one hand, the string theory describes the conductor response with length (L) by its basic properties including the tensile strength (T) and mass (m_c); neglecting the flexural rigidity (EI). On the other hand, the beam theory considers the conductor's vibration response based on its structural properties, including EI. The natural frequencies (f_n) of a vibrating conductor at different free-vibration modes (n) can be calculated when considered as a string or beam using equations (1) and (2), respectively [15].

$$f_n = \frac{n}{2 \times L}\sqrt{T/m_c} \tag{1}$$

$$f_n = \frac{n}{2 \times L}\sqrt{\frac{T}{m_c} + \left(\left(\frac{n \times \pi}{L}\right)^2 \times \frac{EI}{m_c}\right)} \tag{2}$$

The OHL conductors have been modelled using the homogeneous beam theory to study their vibration-induced bending stresses and strains [16]. Literature has reported that the energy absorption and dissipation of complex sandwich structures undergoing vibrations is highly influenced by the composition material properties and dimensions of the outer layers and core [17]–[23]. It has also been reported that sandwich beams are generally more effective than homogenous ones on reducing vibrations [18]. In fact, vibration waves and associated energy losses in sandwich beams have resulted in a distinct behavior categorized by the frequency-dependent stiffness and mass, as illustrated in [20]. Furthermore, it has been observed in [20], [24] that both the stiffness and mass dictate the beam vibration response in different frequency ranges. Therefore, it is more appropriate to consider the conductor's materials and geometry in vibration studies to overcome the simplifications of the homogenization of the complex conductor structure.

B. STANDARD CALCULATIONS OF CONDUCTOR VIBRATION FATIGUE

The existing literature has provided analytical and hybrid (i.e. semi-analytical) models [25], [26] to predict vibration fatigue based on homogenous beam, rod, and rope [27], [28], but none of which gained industry's approbation. The Poffenberger-Swart (P-S) formula shown in (3) is the common practice that has been adopted by IEEE since the 1960s [13], [29], [30]. The P-S formula had been derived by simplifying the conductor to a homogenous cantilever beam with a horizontal tensile load that is exposed to a forced vertical load-induced displacement on its tip causing the bending motion. The P-S computes the maximum bending stresses (σ_a) by defining the conductor tension (T), bending stiffness (EI), and the maximum bending amplitude (Y_b) measured at a distance (x=89mm) from the contact of the clamp with the conductor on the span.

$$\sigma_a = \left(\left(\frac{E_{al} \times d \times T}{EI}\right)/4\left(e^{(-\sqrt{T/xEI})} - 1 + \sqrt{T/xEI}\right)\right) \times Y_b \tag{3}$$

The conductor's bending stiffness (EI) (also known as flexural rigidity) is a measure of its strength and defined as the product of the material's Young modulus (E) and the conductor geometrical moment of inertia (I). Calculating EI has been

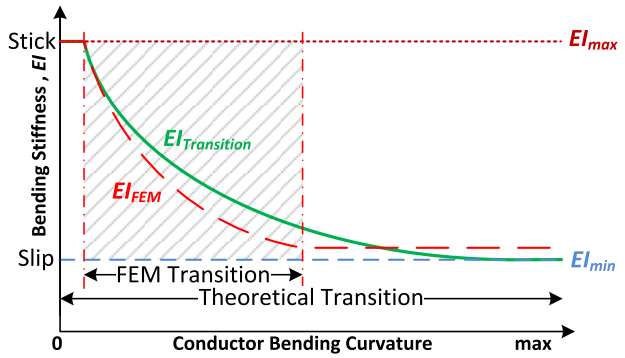

FIGURE 1. Fixed and transitioned bending stiffness modelling hypotheses.

a major concern to engineers when modelling the dynamics of conductors in motion. There have been many experiments performed, and models derived to determine the value of EI [31]–[33]. The interaction between the individual wires of a helically twisted conductor defines its bending response. There are three hypotheses to calculate EI, as summarized in Figure 1. The first two, EI_{min} and EI_{max} (in Figure 1), consider the bending motion of the conductor strands assuming constant value independent of conductor bending curvature, while the third method, $EI_{Transition}$ (Figure 1) considers the tension variation between the strands as a function of conductor bending [34]. In Figure 1, a stranded conductor in motion imposes a shift from the stick-state (i.e., EI_{max}) until the conductor reaches its full slip-state (i.e., EI_{min}) as defined by the theoretical transition ($EI_{Transition}$). There are yet no analytical models that capture this transitional effect. Therefore, more advanced modelling techniques are required to predict the effective transition of the motion between the strands. This is implemented by FEM modelling as FEM transition zone, EI_{FEM} in Figure 1. Consequently, FEM captures the mechanical inertia during the conductor motion, due to the movement between the strands. This is evident from the small bending curvature that the conductor maintains where the stick-state and the slightly higher than the slip-state bending stiffness it maintains at large curvatures, which is not expected due to the surface friction between the strands.

The existing standard practices calculate the induced aeolian vibrations fatigue stresses using EI_{min} [35]. In small vibration amplitudes (high frequencies), there is no slipping between the strands. Thus the rigid beam assumption using EI_{max} can be implemented. However, the effect of tangential compliance reduces the expected EI value to lower than the obtained EI_{max} assumed value [36]. The diverse results on experimentally measured EI indicate that the position of measurement and the OHL span arrangement are crucial [31]–[33]. This endorses the fact that EI is a complex conductor property that depends on the bending strength of the conductor, position of measurement on conductor span, level of vibration amplitudes, and tension variation within the strands. To avoid this complexity, current practices assume a constant value of EI_{min} [34], [36].

TABLE 1. Material properties coefficients for CIGRE safe border line.

Conductor Size Category	Number of Vibration Cycles, Ni	
	$< 2 \times 10^7$	$> 2 \times 10^7$
Single Layer	A = 730 and B = -0.2	A = 450 and B = -0.2
Multi-Layer	A = 430 and B = -0.17	A = 263 and B = -0.17

C. MODELLING METHODS FOR ESTIMATION OF CONDUCTOR LIFETIME

The simplest method to perform stress-life calculations to predict the structural vibration fatigue stresses is the so-called Basquin model [37]. This model forecasts the stress damage for the applied vibration cycles (N_i) to determine the S-N curve using the classical expression in (4), utilizing the exponent (b) for different materials. Other lifetime prediction modelling approaches implement the strain-life fatigue method to estimate the lifetime using the calculated maximum bending strain (ε_a) of the structure. Such a method is well-established by the Coffin-Manson model [38], which consider the plastic deformation (ε_i) of different metallic alloys using the exponents (b) and (c), as expressed in (5).

$$\sigma_a = \sigma_i \times (2N_i)^b \tag{4}$$

$$\varepsilon_a = \frac{\sigma_i}{E} \times (2N_i)^b + \varepsilon_i \times (2N_i)^c \tag{5}$$

The conductor failure due to vibration fatigue can be obtained using the CIGRE criterion introduced in [26], which considers the failure occurring when experimentally three or 10% of the total aluminum wires break, whichever proportion is greater. This experimental approach is expressed by (6) and is often referred to as CIGRE Safe Border Line (CSBL) to determine the conductor's lifetime cycles. Due to the complexity and high cost of conducting such experimentations, the CSBL has been established -so far- for conventional aluminum and aluminum alloys [39]. There are yet no recommendations for all OHL conductors, including the novel HTLS technologies.

$$\sigma_a = A \times (N_i)^B \tag{6}$$

The endured stresses (σ_a) by the conductor are determined when the conductor undergoes a bending motion for a number of cycles (N_i). The A and B coefficients in (6) are determined based on the conductor material properties which are recommended by CIGRE as tabulated in Table 1. The two coefficients (A and B) in (6) are found by fitting the mean of the experimental fatigue test data, as described in [40].

D. REVIEW OF CONDUCTOR GEOMETRY MODELLING EFFORTS

Few studies, such as those conducted by [41], [42], attempted modelling the complex structure of the conductor using, for example, axially loaded beam and relying on the homogeneous beam theory in the early works on FEM analysis. Some other studies implemented the homogenization of the core strands and aluminum layers using an equivalent virtual material that represents the composite conductor

design [43], [44]. Such simplified homogenized approaches neglect the conductor's interstitial interactions.

One of the most recent computer modelling attempts considers conductor complex geometry by using the beam-to-beam contact elements in ANSYS [38]. Others introduced an elasto-plastic numerical FEM approach to model round-strand shaped conductors [45]. It aimed to model the helically twisted conductor strands when undertaking a quasi-static axial load. The vast majority of the reported models in literature have focused on the mechanical performance of conductors with interest in their sizes but not their technologies nor their stranding patterns. Unlike the presented work in this paper, the existing conductor modelling and simulations have not considered the novel conductor designs that have various geometrical shapes and material properties.

E. NEW ERA OF OHL CONDUCTOR TECHNOLOGIES

The advancement in designing and manufacturing OHL conductors have continuously progressed to increase the flexibility of the OHL systems. Monometallic conductors such as All Aluminum Alloy Conductors (AAAC) have replaced the bi-metallic Aluminum Composite Steel Reinforced (ACSR) conductors to increase the power flow within the OHL power corridors. However, such bi-metallic conductors have become the most favorable choice in the industry to increase conductor strength and resolve sag-clearance issues. The steel core in ACSRs increases its mechanical strength while the aluminum increases its electrical conductivity.

Manufacturers have produced novel conductor designs equipped with non-steel core and possibly non-round aluminum strands with some examples shown in Figure 2. In the next subsections, a summary of the commercially available and most-employed conductor technologies is presented.

1) COMPACTION OF ALUMINUM USING TRAPEZOIDAL STRANDS

In an attempt to increase the conductor current carrying capacity, the aluminum part of the conductor is manufactured using trapezoidal-wires (TW) that have replaced classical round-shaped wires. The TW design features compaction of more aluminum wires within the same diametrical cross-section of that equivalent to round-wire (RW) design. Therefore, the compact TW design occupies more conductive material within its cross-section. The downside of this compaction is the reduced resistance that might cause some cooling mechanism issues [10].

2) ENHANCED CONDUCTIVITY BY FABRICATING NEW MATERIALS

Conductor manufacturers have introduced an upgraded class of conventional ACSRs using the aluminum annealing process to produce the Aluminum Conductor Steel Supported (ACSS) conductors (Figure 2). The ACSS conductor design is featured with annealed aluminum strands, which is weaker than the hard aluminum in ACSRs. The annealing process elongates the conductor strands permanently to shift the mechanical strength of the aluminum to its steel core.

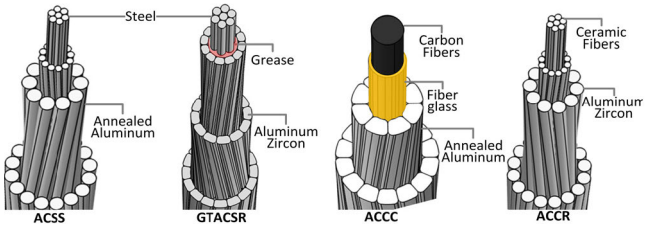

FIGURE 2. Geometries and materials of new conductor technologies.

To overcome the problem of the weaker annealed aluminum in ACSS, conductor manufacturers introduced another class of ACSRs using the Gap Technology to form the Gap Technology of ACSR (GTACSR). This conductor uses aluminum-zircon (AZR) to increase further the annealing temperature of the aluminum strands. The presence of the Gap in between the steel core and aluminum layers for GTACSR design requires a special installation procedure that involves wrapping the aluminum strands around the tensioned steel core. Within this process, conductive grease is applied to reduce the friction between the steel core and aluminum wires.

3) EQUIPPING THE CONDUCTOR WITH NON-METALLIC CORE

The conductor manufacturing process has further evolved to introduce technologies that enable replacing the heavier in weight steel core with a composite material one. This way, the conductor has lower thermal expansion and stronger but lighter core compared to conventional steel. One of the well-known conductor technologies under this category is the Aluminum Conductor Composite Reinforced (ACCR), which is equipped with a composite ceramic conductive core (Figure 2). Like GTACSR, it uses AZR for its outer aluminum layers.

Another novel conductor within this category is Aluminum Conductor Composite Core (ACCC). This conductor comprises a composite carbon fibers core to reduce the weight of the conductor further and achieve lower thermal expansion. As shown in Figure 2, ACCC is equipped with annealed aluminum trapezoidal conductive strands, similar to the ACSS design. The carbon fibers are bounded by a protective shell of glass fibers to prevent corrosion issues.

III. FINITE ELEMENT MODELLING OF CONDUCTOR VIBRATIONS AND FATIGUE STRESSES

The general concept of the proposed FEM approach for assessing the conductor free vibrations and forced vibration fatigue stresses is summarized in the flowchart depicted in Figure 3, highlighting its major computation steps. In Figure 3, the *Input Data* of the FEM consider four main elements: (i) conductor design, (ii) OHL environmental conditions, (iii) installation method, and (iv) operating conditions. The latter three define the implemented Multiphysics and

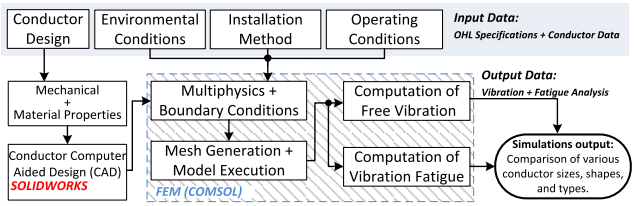

FIGURE 3. Computation steps of proposed FEM approach.

boundary conditions. The *Conductor Design* step requires identifying the mechanical and material properties of the conductor composition, including its stranding pattern to construct its geometry based on the supplied manufacturer data.

The FEM approach in Figure 3 entails creating the conductor's Computer-Aided Design (CAD) in SOLIDWORKS based on the conductor manufacturer data. Therefore, the two-dimensional design of the conductor geometry is created in SOLIDWORKS and extruded in COMSOL to perform the vibrations studies. The conductor can also be formed in COMSOL. Still, SOLIDWORKS is mostly preferred to achieve more design flexibility and accuracy to precisely replicate the design of the conductor geometry as per its manufacturer data.

The designed geometry is imported and discretized (i.e. mesh finite elements generation) in the three-dimensional COMSOL model to perform both the free and forced vibration studies, separately. The free vibrations of the suspended conductor require the additional span length while the forced vibrations have a fixed length as used by the standards and hence can also be used to study conductor fatigue stresses, taking into account the inner and outer strands for various conductor sizes. It is worth mentioning that the forced vibration model can be expanded to execute the stress-life studies as well.

The forced vibrations for calculating conductor fatigue stresses require modelling the mechanics and kinematics of the helically stranded conductor geometry undergoing a bending motion. This FEM fatigue modelling is a complicated endeavor that involves many modelling assumptions to be realized, which are summarized in the next subsection. The computation steps in Figure 3 are detailed next, including the conductor CAD, boundary conditions, and discretization.

A. FEM MODELLING ASSUMPTIONS

1) CONDUCTOR STRANDS SURFACE CONDITIONS

For long-serviced OHLs, conductors can experience cracks, oxidation, fretting wear, tribological layers, and other surface damages associated with vibration fretting and fatigue. Considering such weariness on the conductor surface condition is complex, and hence the proposed model does not consider such wear effects. Furthermore, the wind-induced excitation frequency is used to mitigate the fretting and fatigue wear effects. Therefore, the proposed FEM approach assumes a purely metallic unlubricated surface. Nonetheless, some studies have shown that this conductor-surface condition is not significant near the clamp where the bending stresses are measured [46], [47].

2) INTERSTITIAL INTERACTIONS BETWEEN CONDUCTOR STRANDS

The coefficients of friction between the strands' contact surfaces are a function of many variables such as surface smoothness and existing of fragments due to wires contacting surfaces phenomenon (e.g. corrosion, metal degradation, and cracks). Due to the limited data and studies to obtain such data, the friction coefficients are assumed to be constant and do not change with the mechanical load. This assumption is considered along with the inter-layer strand contacts by creating contact pairs between the strands' surfaces. It must be emphasized that the contact stiffness is assumed constant and changes only with the strand material.

3) CONDUCTOR LENGTH SEGMENTATION

The conductor's sag angle is neglected when executing the bending motion of the conductor geometry. This is because a short portion of the conductor is considered in the executed forced vibrations. However the sag angle can be modelled in the full conductor span for the free vibrations study.

B. DESIGN OF THE REAL CONDUCTOR GEOMETRY

The design of the conductor's real geometry requires developing the CAD modelling of the outer and inner conductor strands. SOLIDWORKS is utilized to create the conductor design based on the supplied data for the conductor geometry dimensions from the manufacturer's datasheet. In the presented work, the two most common conductor stranding shapes are considered: (i) round wire (RW) and (ii) trapezoidal wire (TW) designs.

The design of the RW conductors uses the circle shape to create the round cylindrical wires for the conductor layers. The number of RWs is specified for each layer with rational adjustment of the wires altogether. However, some gaps might become present in the outer layer of the designed conductor geometry. To constrict the conductor RWs, the center of the outer layer wires are connected with a line, as seen in Figure 4 (top). This practice maintains the wires dimension ratio to form constricted strands that are held firmly, as in the real conductor design.

For the TW conductor design, the challenge is to replicate the smooth edge cuts of the trapezoidal-shaped wires. Therefore, it is not a straightforward design as it is the case for RW conductors. To overcome this complexity, the sharp edges of the trapezoid offered in SOLIDWORKS are smoothened by creating virtual circles on its four corners and with radius r_t, as seen in Figure 4 (bottom). The condition that ensures a proper r_t for the different TW sizes is achieved by varying r_t until the sum of the removed top-left area (A_{TL}) and bottom-left area (A_{BL}) is equal to half of the total area (A_{sum}). Fulfilling this condition ensures that the TW strand shape is replicated based on the conductor's manufacturer's specifications.

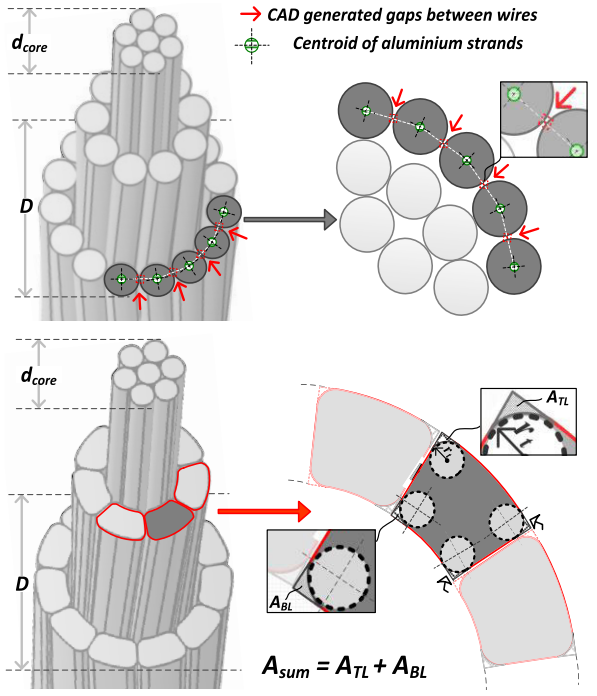

FIGURE 4. Design of RW (top) and TW (bottom) conductor geometries.

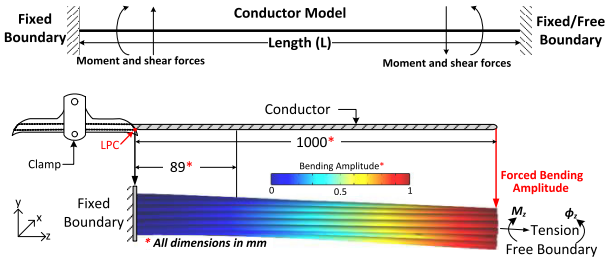

FIGURE 5. Modelling the boundary conditions for the free-vibration of conductor span and vibration fatigue of conductor section.

C. CONDUCTOR GEOMETRY CONFIGURATION

The proposed model considers designing the real helically stranded conductor geometry. This is done with the aid of CAD tools such as SOLIDWORKS, for more flexibility. Then the designed two-dimensional conductor geometry is imported into COMSOL to create the three-dimensional helically twisted stranded layers, as shown in Figure 5.

Each wire in the conductor's layers is generated as a three-dimensional extrusion of the designed two-dimensional wire shape surfaces (e.g. circular or trapezoidal). The extrusion process of the conductor wires is performed along the core centroid axis with the lay length and lay angle being specified for the length of the conductor geometry. For every single wire, the lay length is generated as a solid element and rotated by an angle to match and fit the previously laid length. The same procedure is recapitulated to produce the different conductor designs of the RW and TW conductors. The material properties assigned to the conductor wires after the design is complete. Thus a conductor can represent an ACSR or an AAAC based on material properties used.

D. CONDUCTOR BOUNDARY CONDITIONS

The boundary conditions are very critical when modelling using FEM. For the study of the free vibrations, the boundaries at both ends of conductor are selected to be fully-fixed resembling a rigid clamping mechanism, as considered in the experimental studies [48]. The fully-fixed boundaries constrain the degrees of freedom (DoF) at both ends of the conductor and in all directions. The conductor ends undergo a tensile force with DoFs limited to the horizontal axis while its orientation is restricted except for the horizontal axis. This way, the conductor free vibration frequencies at the different vibration modes of the modelled geometry can be obtained and therefore compared against the analytical solution based on equations (1) and (2). The boundary conditions can also be fixed-free, as shown in Figure 5 (top) to accommodate the flexible end clamping mechanism. However, due to the limitations of the proposed model, the fully-fixed boundary conditions are assigned.

For the study of the forced vibrations, the standard practice of measuring the bending stresses is replicated based on equation (3). Therefore, the three-dimensional conductor geometry is designed as an assembled geometry that is rigidly fixed from one side and subjected to a bending force on the free end, as depicted in Figure 5 (bottom). The assembled conductor geometry has an active length of 1000 mm where the conductor bending vibration fatigue is simulated at 89 mm from the LPC as indicated on the conductor geometry in Figure 5 (bottom).

The fixed and free boundaries at the geometry ends are fully coupled, considering that the conductor layers move independently and interact against each other with longitudinal and crossover contact surfaces. For the fixed-boundary side in Figure 5, the degree-of-freedom (DoF) for the prescribed displacement (Y_b) and center of rotation (Φ) around each strand centroid are constrained in all directions via a rigid connector. The free boundary is subjected to an axial tensile force with the moments (M) and rotation axis DoFs limited to the horizontal axis (z-axis) with a prescribed Y_b while restraining the prescribed, in the solid mechanics physics, moments (i.e. $M_x = M_y = 0$, $M_z \neq 0$) and orientation (i.e. $\Phi_z \neq 0$, $\Phi_x = \Phi_y = 0$) in the remaining axis. The prescribed amplitude is defined as a vertical displacement entered in the input of solid mechanics physics in COMSOL.

E. CONDUCTOR GEOMETRY CONTACT SURFACES AND MESH ELEMENTS GENERATION

The strands in a helically twisted conductor geometry are adjacent to each other forming longitudinal contact surfaces within the same layer and crossover contact surfaces between the different layers. To capture this effect correctly, COMSOL requires modelling the conductor as an assembly, which will allow the modular analysis to automatically assign the pre-simulation contact pairs as *Identity Pairs* for surfaces that are already in contact, as demonstrated in Figure 6. However, the bending motion of the conductor might force some of the non-touching surfaces to become in contact during

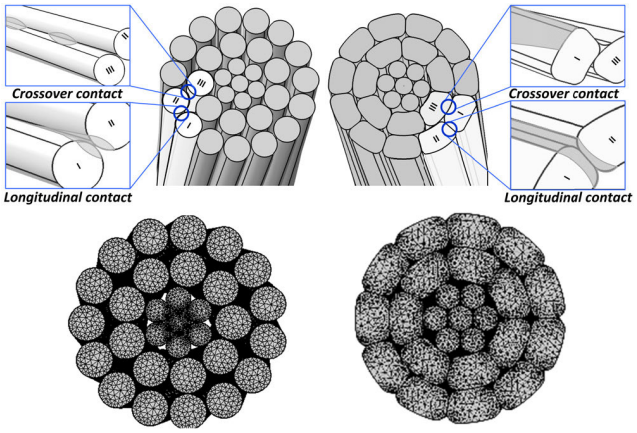

FIGURE 6. "Assembly and mesh" generation in COMSOL for longitudinal and crossover inter-layer contact surfaces of RW and TW strands.

TABLE 2. Properties of ACSR Ibis used in the free vibrations study.

Conductor	ACSR Ibis		
Stranding Pattern	26 Al/ 7 St		
Diameter (mm)	19.88		
Mass (kg/m)	0.813		
Modulus of Elasticity (GPa)	69.8 (AL), 200 (core)		
Rated Breakage Strength (kN)	70.2		
Applied Tension (kN)	15.86		
Test Span Length (m)	13.385	32.3	65.335

the simulations. These ''during-simulation'' contact surfaces are assigned manually between the wires as *Contact Pairs* in COMSOL before running the simulations.

The discretization of the conductor geometry elements is critical for generating its physical mesh size elements. Each wire in the conductor layers is discretized as a solid geometry element to account for the locally formed deviations. The interaction between the individual wires must be accurately captured when creating layer-to-layer contact pairs. The basic solid element properties are defined in COMSOL by the wire radius (r), Young modulus (E), and Poisson ratio (υ). Additionally, the lay length and lay angle are properties primarily considered in this study. However, these have been reported to create a negligible effect on the deformation of the conductor geometry for lay angles below 15° [49]. This step is heavily reliant on the computer capabilities, especially when very fine geometry meshing of the finite elements is required as it is the case when considering the interstitial inner interaction within the bending of conductor geometry.

The mesh size has been defined manually with a maximum element size of 3.68mm, minimum element size of 0.0368mm, curvature factor of 0.2, and the resolution of narrow regions factor of 1. This achieves high accuracy with more than 35 circumferential finite elements being generated for each strand of the RW and TW, as seen in Figure 6.

IV. CONDUCTOR FREE VIBRATION ANALYSIS – HOMOGENEOUS VS. COMPLEX STRUCTURE

The FEM model is initially executed to study the free vibration of composite conductors. The model is validated for the conductor given in Table 2 by computing the natural conductor frequencies (f_n). The feasibility of the model is carried out with the simulations extracted and compared against experimental data and theoretical calculations.

TABLE 3. Natural vibration frequencies for ACSR Ibis in Hz.

Mode No.	Conductor Tension = 22.6%				
	Experimental [48] (f_{Ex})	Analytical Eqn. (2) (f_n)	COMSOL (f_{FEM})	Error, Δf(%)	
				f_{Ex} - f_{FEM}	f_n - f_{FEM}
Span Length = 13.385m					
1	5.2200	5.2185	5.2485	0.5460	0.5749
2	10.4603	10.4376	10.4450	0.1463	0.0709
3	15.6638	15.6579	15.475	1.2053	1.1681
4	20.9681	20.8801	21.262	1.4017	1.8290
5	26.1545	26.1046	25.5290	2.3916	2.2050
Span Length = 32.3m					
1	1.7813	1.7762	1.7810	0.0168	0.2702
2	3.5312	3.5525	3.5321	0.0255	0.5742
3	5.2812	5.3289	5.2941	0.2443	0.6530
4	7.0312	7.1054	7.0332	0.0284	1.0161
5	8.800	8.8821	8.7850	0.1705	1.0932
Span Length = 65.335m					
1	1.1250	1.0688	1.1203	0.4178	4.8185
2	2.0938	2.1375	2.0876	0.2961	2.3345
3	3.1562	3.2063	3.1484	0.2471	1.8058
4	4.2500	4.2751	4.2378	0.2871	0.8725
5	5.2812	5.3439	5.2785	0.0511	1.2238

A. VALIDATION WITH EXPERIMENTAL DATA

The FEM model is examined on ACSR Ibis (Table 2) using the experimental data reported in [48]. The COMSOL simulations used the fully-fixed boundary conditions (in Figure 5), to compare the simulation results with the experimental data. The simulations are also compared against the analytical calculations expressed by (2) for the natural frequencies of the homogeneous beam theory.

The free vibrations analyses are performed for the ACSR Ibis using span lengths of 13.385 m, 32.3 m, and 65.335 m. The experimental data on ACSR Ibis conductor is obtained from [48], which was vibrated via an impact hammer system. Five accelerometers were used to record the natural frequencies along the conductor span (L) located at $L/2$, $3L/8$, $L/4$, $L/8$, and $L/16$. The recorded natural frequencies for the first five modes are listed in Table 3. These values are compared against the analytical calculations and the FEM simulation outputs in the same table.

It is evident that COMSOL outputs (Table 3) are in good agreement with the experimental data with a maximum error of 2.39%. The simulation results are also corroborated with the analytical results with a maximum difference of 4.82%, which occurs at the longest conductor span length. The discrepancies found are attributed to the sensitivity of the boundary conditions of the conductor within the FEM model. The error increases with the increase in span length where the vibration frequencies (f_{FEM}) for the fifth mode reduced from 25.5290 Hz to 5.2785 Hz. The vibration at the low frequencies is more difficult to simulate and introduce more complexities within the model.

B. FREE VIBRATION OF CONDUCTOR WITH VARIOUS MATERIAL COMPOSITIONS

The free vibrations analyses are established for various combinations of the conductor core and aluminum materials and

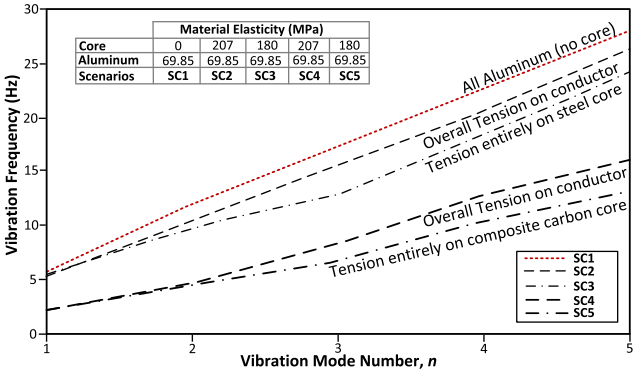

FIGURE 7. Calculated free vibration response on a 13.385 m conductor span with different materials and tension distributions.

tensions. The analyses are carried out for five scenarios (SCs) referred to as SC1, SC2, SC3, SC4, and SC5. The SC1 uses all aluminum alloys and tension applied (22%RBS) to the whole conductor. For SC2, an ACSR steel core is modelled with the tension applied to the entire conductor as well. In SC3, the steel core is replaced with a single composite carbon fibers (CF) rod using properties retrieved from ACCC datasheet. The SC2 and SC3 simulations are re-executed when the tension (22% RBS) is entirely carried by the core and indicated in Figure 7 as SC4 and SC5.

The results of SC2 in Figure 7 show that the vibration of composite conductors consisting of different core and aluminum material properties is not similar to the homogeneous all aluminum (SC1). The material properties and applying tension to the core and aluminum both affect the conductor vibration response. It is observed, from SC1 to SC3, in Figure 7 that the higher the difference between the core and aluminum elasticities, the higher the reduction in vibration frequencies. Thus, the reduction becomes more prominent in SC3 with the composite CF core (ACCC) exhibiting better vibration response.

It is also observed from SC4 and SC5 that there is a further reduction in conductor vibration frequencies when the core carries the conductor tension entirely. This is attributed to the expected inner interaction at higher frequencies. This fact is not valid at lower frequencies, where higher amplitudes are expected, which might affect the accuracy of the model to capture the low frequencies response. Nevertheless, it is not always correct to assume that the OHL conductor acts homogeneously, as evidenced by this analysis. Attention must be paid to the conductor's type and installation conditions when assessing its vibration response.

V. VIBRATION FATIGUE STRESSES ANALYSIS ON MULTI-LAYER OHL CONDUCTORS

The FEM approach is implemented to predict the bending stresses and assess the impact of the cyclic bending loads on the conductor. The analyses here consider the conductors listed in Table 4 with the conductors tensioned at 15% and 35% RBS, respectively.

TABLE 4. Properties of ACSR Raven, Flicker, and Bersfort.

Conductor		ACSR/RW						ACSR/TW	
		Raven		Flicker		Bersfort		Flicker	
Stranding Pattern		1 / 6		7 / 24		7 / 48		7 / 18	
RBS (kN)		19.5		140.1		180.1		76.50	
Diameter (mm)		10.11		21.49		35.6		19.71	
Mass (kg/m)		0.216		1.628		2.37		0.912	
Conductor Layer		No. of Strands and lay angle							
Core	1st	1	0	1	0	1	0	1	0
	2nd	-	-	6	5.8°	6	6.2°	6	5.8°
Aluminum	1st	6	6°	9	10.7°	10	9.7°	7	10.7°
	2nd	-	-	15	12.9°	16	10.7°	11	12.9°
	3rd	-	-	-	-	22	11.7°	-	-

TABLE 5. Material properties for studied ACSR conductors.

Conductor Property		ACSR/RW			ACSR/TW
		Raven	Flicker	Bersfort	Flicker
Young modulus (MPa)	Outer-layer	69850	69850	69850	69850
	Core	207000	207000	207000	207000
Poisson ratio	Core	0.3	0.3	0.3	0.3
	AL	0.33	0.33	0.33	0.33
Bending Stiffness (N-m^2)	EI_{min}	3.95	54.45	61.63	-
	EI_{max}	25.18	15.77	38.27	-
Composition Category		*Single-Layer*	*Two-Layer*	*Three-Layer*	*Two-Layer*

The selection of these conductors (in Table 4) is intended to evaluate the capability of existing fatigue calculation methods, based on the P-S formula (3), in determining the effect of composite conductor properties instead of the homogeneous assumption. The calculated bending stiffness in Table 5 is not calculated for ACSR/TW because the standard equations (EI_{min} and EI_{max}) are only capable of calculating ACSR/RWs. The studied ACSR conductors are ACSR/RW Raven (single-layer), ACSR/RW Flicker (two-layer), ACSR/RW Bersfort (three-layer), and ACSR/TW Flicker (two-layer). The fatigue stresses are calculated for a forced bending amplitude in the range of 0 – 1 mm when the conductors are subjected to tensile forces of 15% and 35% RBS.

A. SINGLE – LAYER ACSR CONDUCTORS

Figure 8 illustrates the fatigue stresses against the forced bending amplitudes for the single-layer and multi-layer ACSRs. The simulation outputs indicate a good agreement of FEM with the P-S solution for the single-layer ACSR, which is in line with the EI_{min} hypothesis. This is true for both tensions (15% and 35% RBS) in Figure 8 indicating that the assumption of linear behavior of EI for single layer conductor structures is a valid approximation.

B. TWO – LAYER ACSR CONDUCTOR

The two-layer ACSR conductors adopt a more complex bending behavior, which is also dependent on the conductor tension. From Figure 8, it is evident that fatigue stresses on the two-layer Flicker at 15% RBS cannot be predicted using the P-S formula with either EI_{max} or EI_{min}. In fact the FEM outputs indicate that Flicker's fatigue is somewhere in between of these two (EI_{max} and EI_{min}) curves and it is dependent on the tension of the conductor. This is a sensible conclusion

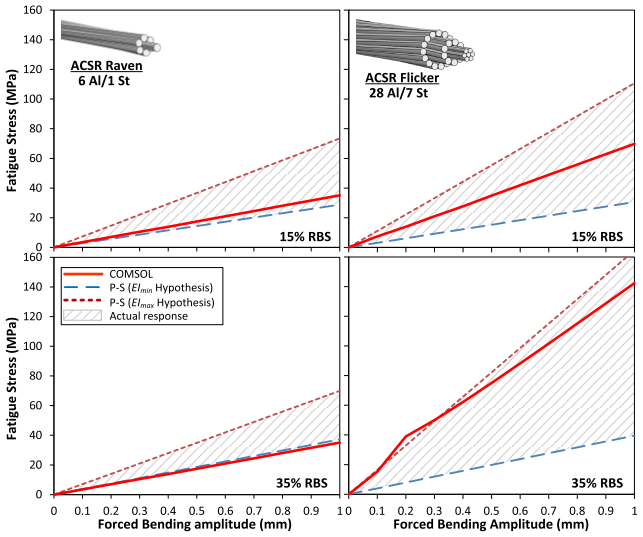

FIGURE 8. Fatigue stresses of the outermost aluminum layer for single-layer ACSR Raven and multi-layer flicker at 15%RBS and 35%RBS.

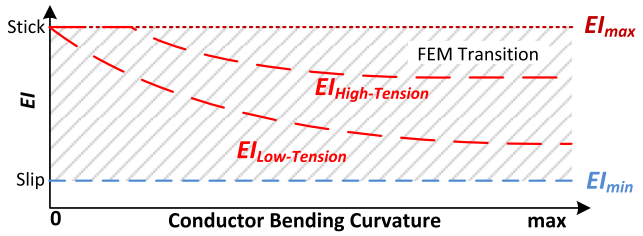

FIGURE 9. FEM transitioned bending stiffness for low and high tensions.

as the increase in tension ''interlocks'' the aluminum strands of the different layers making it to respond nearer to the P-S formula with the EI_{max} hypothesis.

By observing the two-layer aluminum conductor fatigue stress response in Figure 8, it can be seen that at least for the 35% RBS tension, small bending amplitudes (up to 0.2 mm) result in a conductor behavior similar to the homogeneous assumption response. This is not observed when the 15% RBS tension is modelled. Thus, it indicates that the bending stiffness is also affected by the tension attributed to the shift of stresses to the inner layers as the tension is increased. Furthermore, there is a finite value of bending curvature that the conductor's integrity is maintained by the helically wrapped strands inward forces, which are increased at higher conductor tensions. In Figure 9, the EI_{FEM} indicates the complex response of bi-metallic conductors' vibration and the interaction between the conductor layers. This is captured by the FEM simulations evidenced by the dynamic fatigue strain response in Figure 8. The next step is to investigate the more complex case of three-layer ACSRs, as discussed in the following subsections.

C. TRIPLE – LAYER ACSR CONDUCTOR

ACSR Bersfort, described in Table 4 and Table 5, is used for modelling the fatigue stresses developed on more

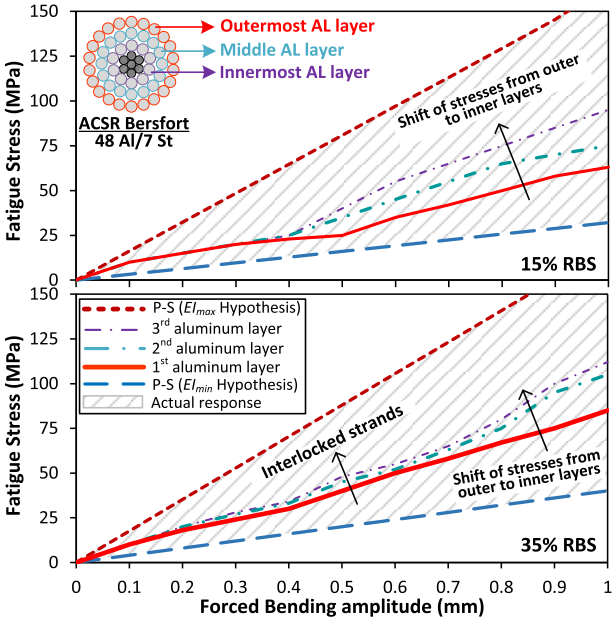

FIGURE 10. Fatigue stresses for Bersfort: 15% and 35%RBS.

complex larger ACSR conductors. The simulation results in Figure 10 endorses similar non-linear fatigue stresses with the previous two-layer bi-metallic conductor. The effect on conductor complexity and tension indicate fatigue stresses that lay between both hypotheses (EI_{min} and EI_{max}).

In Figure 10, the fatigue stresses of individual aluminum layers is calculated. Again the EI_{min} and EI_{max} simplified hypotheses do not capture the actual response of Bersfort for 15% and 35% RBS while FEM simulations can calculate the response of the complex structure. At 15% RBS, the layer stresses (in Figure 10) are lower and almost equal for bending amplitudes below 0.4 mm. The differentiation occurs at higher amplitudes with the innermost layer being the most affected one. Therefore, the assumption of calculating the conductor fatigue stresses using the outermost layer, as in the industry practices, may not capture the actively internal fatigue stresses of the large conductors.

Increasing the tension to 35% RBS, the fatigue stresses increase as it is expected and shown in Figure 10. The fatigue stresses for all layers are very similar. This response indicates that the strands within the different aluminum layers interlock together, i.e., producing an increased contact surface (i.e. larger area of friction) between the adjacent layers. Therefore, the stresses of the outermost layer can be, to some extent, used for the fatigue severity assessment.

D. TRAPEZOIDAL-SHAPE CONDUCTOR STRANDS

Flicker trapezoidal strand equivalent design, described in Table 4 and Table 5, is used to compare the fatigue of round (RW) against trapezoidal (TW) strand shape. In Figure 11, the fatigue stresses for ACSR Flicker are demonstrated for both TW and RW designs when

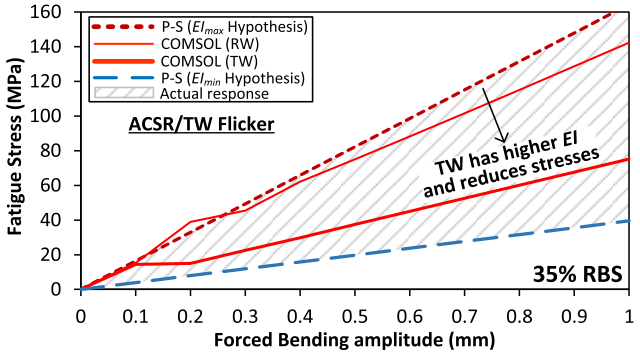

FIGURE 11. Comparison of simulated fatigue stresses of the outermost aluminum layer for ACSR Flicker RW and TW stranding patterns.

applying 35% RBS. The P-S curves are calculated using EI_{min} and EI_{max} round Flicker design and compared to the simulated ACSR/TW.

It is observed that the predicted fatigue stresses of the TW design are lower than that of the RW design. This could be the result of the large contact surface areas between the overcrossing layers of the TW strands that help on dissipating energy in more mass instead of dissipating energy on a smaller elliptical area of the RW design. Therefore, fatigue severity for TWs is diminished on the outermost layer compared to RWs, as evidently shown in Figure 11 and in agreement with the work presented in [38].

VI. CONCLUSION AND SUGGESTED FUTURE WORK

The presented FEM approach in COMSOL along with the modelling assumptions are successfully used to predict the free and forced vibrations performance of OHL conductors. The model is implemented on single and multi-layer ACSR/RW and ACSR/TW conductor to study the effect of conductor design on vibration response. The simulation results of free and forced vibrations for these conductors are summarized as follows:

- Homogeneous AAACs have worse performance than the ACSRs suggesting that the higher the material property differences between the core and aluminum parts, the better the conductor vibration response.
- The higher the tension difference between the core and aluminum, the better the vibration response at higher vibration modes. This implies an interaction between the tensioned core and slack aluminum strands.
- The more aluminum strand layers a conductor has, the better the vibration response. However, it might not always be the outer layer that experiences higher fatigue stresses.
- The flexural rigidity of conductors is complex and it is dictated by the interaction of conductor layers. Hence the shape of the strands affects its value. The best simplification could be to use an average value between the maximum and minimum flexural rigidity values used within the P-S theory.

It is evident that the P-S theory is very simplified to assess conductor vibration-induced fatigue. Subsequently, it is expected to under-estimate the lifetime of OHL conductors, especially on the novel designs that have gained their improved electrical performance based on their increased complexity in design, materials, and installation practices. Consequently, estimating the life expectancy due to vibration fatigue of new conductor designs will require further simulations and experimentation to improve understanding of their structural dynamics.

REFERENCES

[1] J. Dudiak and M. Kolcun, "Integration of renewable energy sources to the power system," in *Proc. 14th Int. Conf. Environ. Electr. Eng.*, May 2014, pp. 148–151.
[2] H. Lund, "Renewable energy strategies for sustainable development," *Energy*, vol. 32, no. 6, pp. 912–919, Jun. 2007.
[3] P. J. Baruah, N. Eyre, M. Qadrdan, M. Chaudry, S. Blainey, J. W. Hall, N. Jenkins, and M. Tran, "Energy system impacts from heat and transport electrification," *Proc. Inst. Civil Eng.-Energy*, vol. 167, no. 3, pp. 139–151, Aug. 2014.
[4] E. Veldman, M. Gibescu, H. Slootweg, and W. L. Kling, "Impact of electrification of residential heating on loading of distribution networks," in *Proc. IEEE Trondheim PowerTech*, Jun. 2011, pp. 1–7.
[5] K. J. Dyke, N. Schofield, and M. Barnes, "The impact of transport electrification on electrical networks," *IEEE Trans. Ind. Electron.*, vol. 57, no. 12, pp. 3917–3926, Dec. 2010.
[6] D. Ciechanowicz, D. Pelzer, and A. Knoll, "Simulation-based approach for investigating the impact of electric vehicles on power grids," in *Proc. IEEE PES Asia–Pacific Power Energy Eng. Conf. (APPEEC)*, Nov. 2015, pp. 1–5.
[7] K. Kopsidas, S. M. Rowland, and B. Boumecid, "A holistic method for conductor ampacity and sag computation on an OHL structure," *IEEE Trans. Power Del.*, vol. 27, no. 3, pp. 1047–1054, Jul. 2012.
[8] K. Kopsidas, M. A. AlAqil, T. Kavanagh, and A. Halder, "Performance and control of vibrations of HTLS conductors," CEATI Publications, Montreal, QC, Canada, TODEM 33106, 2019, pp. 1–83. [Online]. Available: https://www.ceati.com/publications/publication-details?pid=33106
[9] M. A. Al Aqil and K. Kopsidas, "Finite element modelling approach to assess fatigue of composite OHL conductors," in *Proc. IEEE Power Energy Soc. Gen. Meeting (PESGM)*, Atlanta, GA, USA, Aug. 2019, pp. 1–5.
[10] S. A. Rahman and K. Kopsidas, "Impact of simplified convection model in overhead lines thermal rating calculation methods," in *Proc. IEEE/PES Transmiss. Distrib. Conf. Expo. (T&D)*, Apr. 2018, pp. 1–9.
[11] G. Diana and M. Falco, "On the forces transmitted to a vibrating cylinder by a blowing fluid," *Meccanica*, vol. 6, no. 1, pp. 9–22, Mar. 1971.
[12] H. Wolf, B. Adum, D. Semenski, and D. Pustaić, "Using the energy balance method in estimation of overhead transmission line aeolian vibrations," *Strojarstvo*, vol. 50, no. 5, pp. 269–276, 2008.
[13] *Modelling of Aeolian Vibration of Single Conductor: Assessment of the Technology*, document CIGRE SC22 EG22-11, ELECTRA, 1998, pp. 53–69.
[14] *Modeling of Aeolian Vibrations of Single Conductors and Single Conductors Plus Dampers*, document CIGRE WG B2.31, 2011.
[15] A. O. El-Nady and M. M. A. Lashin, "Free vibration analysis of sandwich beam structure using finite element approach," *IOSR J. Mech. Civil Eng.*, vol. 12, no. 6, pp. 34–42, 2015.
[16] *IEEE Guide for Laboratory Measurement of the Power Dissipation Characteristics of Aeolian Vibration Dampers for Single Conductors*, IEEE Standard 664-1993, 1993.
[17] Y. Yang, B. Li, Z. Chen, N. Sui, Z. Chen, M.-U. Saeed, Y. Li, R. Fu, C. Wu, and Y. Jing, "Acoustic properties of glass fiber assembly-filled honeycomb sandwich panels," *Compos. B, Eng.*, vol. 96, pp. 281–286, Jul. 2016.
[18] M. Ruzzene, "Vibration and sound radiation of sandwich beams with honeycomb truss core," *J. Sound Vib.*, vol. 277, nos. 4–5, pp. 741–763, Nov. 2004.
[19] Z. Li and M. J. Crocker, "A review on vibration damping in sandwich composite structures," *Int. J. Acoust. Vib.*, vol. 10, no. 4, pp. 159–169, 2005.

[20] A. C. Nilsson, "Wave propagation in and sound transmission through sandwich plates," *J. Sound Vib.*, vol. 138, no. 1, pp. 73–94, Apr. 1990.
[21] P. Qiao and M. Yang, "Impact analysis of fiber reinforced polymer honeycomb composite sandwich beams," *Compos. B, Eng.*, vol. 38, nos. 5–6, pp. 739–750, Jul. 2007.
[22] M. A. Hazizan and W. J. Cantwell, "The low velocity impact response of an aluminium honeycomb sandwich structure," *Compos. B, Eng.*, vol. 34, no. 8, pp. 679–687, Dec. 2003.
[23] M. He and W. Hu, "A study on composite honeycomb sandwich panel structure," *Mater. Des.*, vol. 29, no. 3, pp. 709–713, Jan. 2008.
[24] J. Zhao, X.-M. Wang, J. M. Chang, Y. Yao, and Q. Cui, "Sound insulation property of wood–waste tire rubber composite," *Compos. Sci. Technol.*, vol. 70, no. 14, pp. 2033–2038, Nov. 2010.
[25] *State of the Art for Testing Self-Damping Characteristics of Conductors for Overhead Lines*, document CIGRE WG B2.25 ELECTRA, 2011.
[26] *Recommendations for the Evaluation of the Lifetime of Transmission Line Conductors*, document CIGRE WG 22.04, ELECTRA, 1979.
[27] W. K. Lee, "An insight into wire rope geometry," *Int. J. Solids Struct.*, vol. 28, no. 4, pp. 471–490, 1991.
[28] M. Giglio and A. Manes, "Life prediction of a wire rope subjected to axial and bending loads," *Eng. Failure Anal.*, vol. 12, no. 4, pp. 549–568, Aug. 2005.
[29] *Guide to Vibration Measurements on Overhead Lines*, document CIGRE SC.22 WG.11, ELECTRA, 1995.
[30] *IEEE Guide for Aeolian Vibration Field Measurement of Overhead Conductors*, IEEE Standard 1368-2006, 2006, pp. 1–35.
[31] K. O. Papailiou, "On the bending stiffness of transmission line conductors," *IEEE Trans. Power Del.*, vol. 12, no. 4, pp. 1576–1588, Oct. 1997.
[32] K. G. McConnell and W. P. Zemke, "The measurement of flexural stiffness of multistranded electrical conductors while under tension," *Exp. Mech.*, vol. 20, no. 6, pp. 198–204, Jun. 1980.
[33] T. O. Seppa, "Measurements of bending stiffness of transmission conductors in the free span and near the ends of the span," in *Proc. Presentation CIGRE*, Paris, France, 1995, Paper SC 22 WG 11.
[34] F. Kiessling, P. Nefzger, J. F. Nolasco, and U. Kaintzyk, *Overhead Power Lines: Planning, Design, Construction*. Berlin, Germany: Springer, 2014.
[35] *EPRI Transmission Line Reference Book: Wind-Induced Conductor Motion*, EPRI, Palo Alto, CA, USA, 2006.
[36] C. Hardy and A. Leblond, "On the dynamic flexural rigidity of taut stranded cables," in *Proc. 5th Int. Symp. Cable Dyn.*, Santa Margherita Ligure, Italy, 2003, pp. 45–52.
[37] O. H. Basquin, "The exponential law of endurance tests," in *Proc. Amer. Soc. Test. Mater.*, vol. 10, 1910, pp. 625–630.
[38] S. Lalonde, R. Guilbault, and S. Langlois, "Modeling multilayered wire strands, a strategy based on 3D finite element beam-to-beam contacts—Part II: Application to wind-induced vibration and fatigue analysis of overhead conductors," *Int. J. Mech. Sci.*, vol. 126, pp. 297–307, Jun. 2017.
[39] B. Wareing, *Wood Pole Overhead Lines*. London, U.K.: Institution of Engineering and Technology, 2005.
[40] R. B. Kalombo, J. M. G. Martínez, J. L. A. Ferreira, C. R. M. da Silva, and J. A. Araújo, "Comparative fatigue resistance of overhead conductors made of aluminium and aluminium alloy: Tests and analysis," *Procedia Eng.*, vol. 133, pp. 223–232, Jan. 2015.
[41] M. Kraus and P. Hagedorn, "Aeolian vibrations: Wind energy input evaluated from measurements on an energized transmission line," *IEEE Trans. Power Del.*, vol. 6, no. 3, pp. 1264–1270, Jul. 1991.
[42] O. Barry, R. Long, and D. Oguamanam, "Simplified vibration model and analysis of a single-conductor transmission line with dampers," *Proc. Inst. Mech. Eng., C, J. Mech. Eng. Sci.*, vol. 231, no. 22, pp. 4150–4162, Nov. 2017.
[43] J. Murin, J. Hrabovsky, M. Aminbaghai, R. Gogola, V. Goga, F. Janíček, and S. Kugler, "Modelling and simulation of power lines made of composite structures," *Compos. Struct.*, vol. 183, pp. 286–298, Jan. 2018.
[44] Y. D. Kubelwa, R. Loubser, and P. Moodley, "Experimental investigations of bending stresses of ACSR conductors due to aeolian vibrations," *CIGRE Sci. Eng.*, vol. 9, pp. 17–26, Nov. 2017.
[45] R. Judge, Z. Yang, S. W. Jones, and G. Beattie, "Full 3D finite element modelling of spiral strand cables," *Construct. Building Mater.*, vol. 35, pp. 452–459, Oct. 2012.
[46] G. Qi, "Computational modeling for stress analysis of overhead transmission line stranded conductors under design and fretting fatigue conditions," Ph.D. dissertation, Dept. Civil Eng. Appl. Mech., McGill Univ., Montreal, QC, Canada, 2013.
[47] F. Levesque, S. Goudreau, S. Langlois, and F. Légeron, "Experimental study of dynamic bending stiffness of ACSR overhead conductors," *IEEE Trans. Power Del.*, vol. 30, no. 5, pp. 2252–2259, Oct. 2015.
[48] N. Barbieri, O. H. D. S. Júnior, and R. Barbieri, "Dynamical analysis of transmission line cables. Part 1—Linear theory," *Mech. Syst. Signal Process.*, vol. 18, no. 3, pp. 659–669, May 2004.
[49] S. R. Ghoreishi, T. Messager, P. Cartraud, and P. Davies, "Validity and limitations of linear analytical models for steel wire strands under axial loading, using a 3D FE model," *Int. J. Mech. Sci.*, vol. 49, no. 11, pp. 1251–1261, Nov. 2007.

MOHAMMED A. ALAQIL (Member, IEEE) was born in Al-Ahssa, Saudi Arabia. He received the B.Sc. degree (Hons.) in electrical power systems engineering from Universiti Tenaga Nasional (UNITEN), Malaysia, in 2012, and the M.Sc. degree (Hons.) in electrical power system engineering from The University of Manchester, U.K., in 2015, where he is currently pursuing the Ph.D. degree in electrical power systems engineering. He is a former Electrical Engineer with Saudi Electricity Company. He has been appointed recently as a Visiting Lecturer with the University of Chester. He currently holds a position as a Lecturer with the College of Engineering, King Faisal University, Saudi Arabia. He is a Corresponding Member of CIGRE WG B2.79 and has been engaging in several industrial projects on overhead lines design and optimization in collaboration with CEATI (Canada), National Grid Electricity Transmission (U.K.), and Energy Supply Board International (Ireland).

KONSTANTINOS KOPSIDAS (Senior Member, IEEE) received the M.Sc. and Ph.D. degrees in electrical power systems engineering from the School of Electrical and Electronic Engineering, The University of Manchester, Manchester, U.K., in 2005 and 2009, respectively. He is currently a Senior Lecturer of electrical power engineering with the School of Electrical and Electronic Engineering, The University of Manchester. His research interests include component design aspects and network operation strategies that can improve the resilience and flexibility of electrical power networks. He is an expert in the area of overhead lines and underground cables design modeling and smart grids reliability assessments. He is/has been actively involved with a number of EPSRC, EU, and industrial projects. He is the Convener of a CIGRE WG C4.25, a member of the IEEE Grid Code Task Force, a Consultant for several national and international activities (UKPN, Mott Macdonald, Balfour Beatty), and a member of Advisory Boards of EU Projects (Grid4EU), Quality Assurance Organizations (H.Q.A.A.A.), and Industry (ECOFYS). He has authored or coauthored more than 50 research articles and reports, and has been delivering CPD courses related to OHL in industry and academia.